BASS Measurements of Currents, Waves, Stress, and Turbulence in the North Sea Bottom-Boundary Layer

F. T. Thwaites and A. J. Williams 3rd
Woods Hole Oceanographic Institution

Abstract- **Shallow-water-boundary layers are effected by current, waves, bottom topography, and stratification. Precise turbulence measurements through such regions are difficult. A deployment of a BASS (Benthic Acoustic Stress Sensor) tripod in November 1997 in the North Sea in 15 meters of water provides a data set to examine turbulent boundary layer models. The deployment spanned both calm and storm sea conditions, had strong tidal currents, the location was uniform horizontally, and the bottom-boundary layer was well mixed in temperature. Estimates of stress derived from the covariance, log-fit, drag-law, and inertial-dissipation method have been compared. The covariance stress estimate had the largest sample to sample scatter, but from theoretical considerations should give the best estimate in stratified flow. The drag-law estimate gave the least sampling variability but suffers from the user having to measure a drag coefficient by some other method. The inertial-dissipation method was more tolerant to sensor misalignment, had the second greatest sampling variability, and could not be used to measure stress during slack tide. Averaging many semidiurnal tidal cycles showed greater tidal asymmetry of the log-fit stress than the covariance or inertial-dissipation stress estimates. Turbulent energy generation and dissipation were measured and balanced individually for the upper two sensors and followed a one-over-height-above-bottom profile.**

INTRODUCTION

The measurement in turbulent-boundary layers of stress and turbulent-kinetic-energy generation and dissipation is fundamental to understanding how the ocean works. Bottom-boundary-layer stress is very important in sediment erosion, transport, and deposition. Understanding turbulent-kinetic-energy (TKE) production and dissipation is important in modeling mixing in the ocean of oxygen, heat, waste, and nutrients.

Despite the difficulty in measuring turbulent quantities in the ocean such as shear stress by different methods, many researchers have done so. Bowden and Howe ’63 [1] used electromagnetic flow meters in a tidal estuary to measure the turbulent statistics of the turbulent-velocity correlation function and stress and measured a drag coefficient of less than $3 * 10^{-4}$. The tidal estuary had no waves and may have been stratified. Sternberg ’67 [2] measured the turbulent shear stress by the log-fit method in linear-tidal channels with no waves and measured drag coefficients from $2\text{-}4 * 10^{-3}$. McLean ’83 [3] compared covariance stress and log-fit stress in a bay and found a large amount of scatter and sampling variability. Gross and Nowell ’83 [4] compared log-fit and covariance stress in a channel with linear tides and no waves. They found the log-fit stress exceeded the covariance stress during flow acceleration and deceleration and measured a drag coefficient of $3.8 * 10^{-3}$. Gross and Nowell ’85 [5] compared log-fit, covariance and inertial dissipation stress in two channels with linear tides and no waves. They found the inertial dissipation stress, above the lowest sensor, to be within 20 % of the log-fit stress. Their covariance stress was lower presumably due to the spatial separation of the propeller triplets missing some of the Reynold’s stress. Gross et al ’94 [6] compared inertial dissipation and log-fit stress on the shelf when waves were present. They found the inertial dissipation stress could exceed the log-fit stress when waves were present due to advection of the wave generated TKE up to the sensing volumes. Sanford and Lien ’99 [7] compared log-fit, covariance, and dissipation stresses along with a new stress estimate from the vertical flux of vorticity during ebb tides, with no mentioned waves. They found a two-layer flow where in the lower layer all the stress estimates agreed but in the upper layer the log-fit stress was 3.2 times the covariance stress.

Many researchers have looked into asymmetries in tidal current, stress and TKE. J. Wolf ’80 [8] estimated the bottom shear stress from harmonic analysis of tide gauges and current meters in the Irish Sea and found the bottom stress leads the tidal current. Bowden and Ferguson ’80 [9] measured covariance stress in the Irish Sea and found the drag coefficient to be less during the flow’s deceleration but that the TKE, scaled by mean current squared, showed no hysteresis. Soulsby and Dyer ’81 [10] measured log-fits to a linear tide with no waves and found the stress lags the current with increasing height above bottom and the current at large heights above bottom lags on the accelerating tide. McLean ’83 [3] measured covariance and log-fit stress in a North Sea tidal inlet and found the covariance stress to lag the current significantly at 214 cm above bottom. Gross and Nowell ’83 [4] found in a channel that the shear stress during tidal acceleration was carried by smaller eddies than during deceleration. Gross et al ’92 [11] measured log-fits on the shelf with significant waves and only measured acceleration effects to the log-profiles above 2 meters. Green and McCave ’95 [12] measured the inertial dissipation stress close to the bottom in the Irish Sea with

This work was supported by ONR grant N00014-97-10076.
WHOI contribution number 10,022.

small waves and found no significant tidal asymmetry. Simpson et al '96 [13] measured dissipation in the Irish Sea and found it to significantly lag behind current and that lag increased with height and stratification. They measured a 2-hour lag at 70 meters above bottom in unstratified water and measured a 4-hour lag at 40 meters with a stratified water column. Lueck and Lu '97 [14] made log-fit measurements with an ADCP in a channel with linear tides and no wind or waves. They found acceleration effects to the log profile above 10 meters, and measured a drag coefficient of $9 * 10^{-3}$.

Careful observations are valuable even when they seem contradictory because as our understanding improves, they may be incorporated in the web of evidence that confirms or denies theories. Asymmetries in tidal current and stress are not unexpected. Tidal forcing of a boundary layer is unsteady and the region affected by the boundary grows into the interior of the flow during the acceleration phase of the flow. Measurements near the bed should show less phase lag than measurements farther from the bed. Observations of stress in accelerating flows should be phase delayed while decelerating flows should generally be less influenced by the reduction of friction at the bed. In decelerating flows, turbulence decays by dissipation rather than being supported by reduced bottom friction. Increase in effective friction by surface waves improves communication of stress from the bed into the interior. Most observations since 1980 confirm these summaries. Where there is stratification, the situation is more complex and some observations are in stratified conditions. Stratification is a barrier or attenuator of turbulent exchange and should further retard the phase of stress observations with respect to the tidal forcing. The observations where stratification was known to exist seem to support this.

This paper compares stress from the drag-law, covariance, log-fit, and inertial-dissipation estimates from a Benthic Acoustic Stress Sensor (BASS) deployment in a shallow coastal area. The paper then describes measurements, from the same deployment, of turbulent-kinetic-energy generation and dissipation at two heights above the bottom and compares these measurements to the wall-layer turbulence model.

MEASUREMENTS

A three-sensor BASS tripod was deployed 16 kilometers Northwest of IJmuiden, The Netherlands, from November 11 to December 1 of 1997, as part of the NATO mine burial exercise. The deployment was in 15.6 meters of water in a sandy area that was flat except for sand ripples. There were primarily two length scales of ripples, small ripples of order one or two centimeters high and ten to twenty centimeters apart, and sand waves a meter high several hundred meters apart. The area had strong tidal currents of order 50 centimeters per second and the deployment spanned both calm weather and some storms. During the calm periods, waves were not felt on the bottom and during storms waves reached the bottom. During the deployment, the bottom boundary layer was well mixed in temperature, to the accuracy of the thermistors, about 0.01 degrees Centigrade. Measurements in this unstratified, flat boundary layer are good for comparing to unstratified turbulence models.

The tripod deployed is shown in Fig. 1 and had three velocity sensors, five optical backscatter sensors (OBS), seven thermistors, a pressure sensor, and a conductivity sensor. Additionally the tripod measured tilt and compass heading to enable rotation of measured velocity vectors into earth coordinates. The BASS system was designed to measure the covariance Reynold's stress [15]. The velocity sensors were logarithmically spaced above the bottom with sensor one at 39.4 centimeters, sensor two at 118.7 centimeters, and sensor three at 308.6 centimeters above bottom. The BASS velocity sensors acoustically measure velocity over 15 centimeter measurement paths. Optical

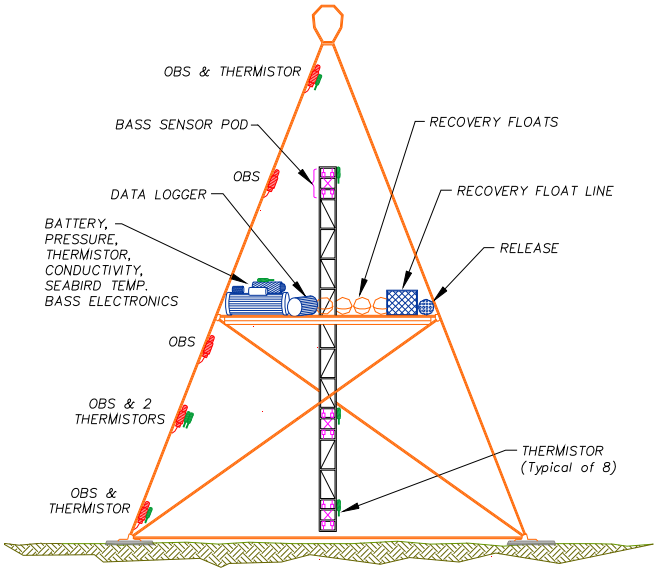

Fig. 1. BASS tripod configuration used the North Sea deployment.

backscatter sensors were located at 0.305, 1.12, 2.01, 2.83, and 4.05 meters above bottom. Thermistors were located 0.305, 0.406, 1.117, 1.213, 2.39, 3.112, and 4.05 meters above bottom. The pressure sensor, Seabird conductivity and temperature sensors were located 2.39 meters above bottom. The data from all the sensors were measured every 0.43 seconds and recorded on a hard disk for processing later.

Typical raw measurements are plotted for a very short time record in Fig. 2. This time record was from a period when swell reached the bottom. The OBS sensors were calibrated in Formazin Turbidity Units from a Formazin standard and not calibrated with the local sediment so no

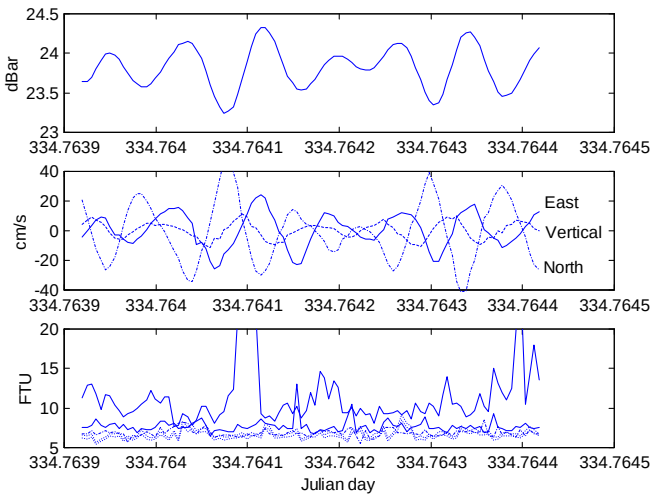

Fig. 2. North Sea BASS short time record of absolute pressure, velocity of sensor three, and optical backscatter at five heights above bottom.

numerical estimate of sediment load can be made. From the raw velocity, stress was calculated by the four estimates and turbulent-kinetic-energy production and dissipation were calculated.

DATA ANALYSIS

After the tripod was recovered, the raw data was analyzed to calculate estimates of stress and turbulence. The quadratic drag-law produced an estimate of stress that had the least sampling variability. In equation (1), τ is the shear

$$\tau = C_d \times \rho \times \overline{U}^2 \qquad (1)$$

stress, C_d is a drag coefficient, ρ is the fluid density, and $\overline{U}$ is the mean velocity at one meter above bottom. The drag coefficient, when waves are not present, is typically between 2-4 * 10^{-3} [2]. When waves are present, the wave boundary layer adds turbulence and turbulent diffusivity in the lower part of the current boundary layer and can increase the drag coefficient to 10*10^{-3} [16]. The difficulty in using the drag-law is determining the drag coefficient, which depends on bottom roughness, presence of waves, and stratification. The drag coefficient, used to compute stress, was computed from a regression between the covariance-stress estimate and current, and was assumed constant for the deployment. Drag coefficient dependence on wave velocity was also computed for half-hour averages and is described below. The drag stress was computed from seven-minute means of velocity that were logarithmically extrapolated to one-meter height. The seven-minute means were then averaged with a one-half hour, zero-phase, low-pass filter. The low-pass filter was a half-hour, two-pole Butterworth filter used on the sequence twice, once in each direction to cancel out phase shifts. This filter was used to produce all the half-hour means from seven-minute means and reduces some of the errors caused by just taking half-hour means of a signal that is not quite stationary over a half-hour.

The covariance stress estimate is a direct measure of one component of the Reynold's stress tensor. In equation

$$\tau_{zx} = -\rho\overline{w'u'} \qquad (2)$$

(2) τ_{zx} is the vertical shear stress, ρ is the fluid density, w' is the fluctuating part of the vertical velocity, and u' is the fluctuating part of the along current velocity. The overbar means a time average. It has been shown by Heathershaw and Simpson [17] that the sampling variability of this measurement is large, real, and inherent to a turbulent flow. This covariance has to be averaged for long periods and is often averaged over several sensors. Seven-minute covariance means were calculated and then averaged with a one-half hour, zero-phase, low-pass filter.

In the presence of waves, the covariance estimate is easily swamped if the attitude (or attitude the velocities are rotated into) is not very accurate. Wave velocities are in quadrature and when wave velocities are much larger than turbulent velocities, inaccuracy in measuring this quadrature can create a bias that can be much larger than the turbulent stress. In this deployment, the bottom was flat, sensor tilt was accurately measured, and tidal currents were usually significantly larger than wave velocities.

The covariance estimate of stress directly measures the velocities of the eddies transporting momentum in the boundary layer. Larger eddies are more effective at transporting momentum, but the eddy size is limited by the eddy's distance from the bottom. Close to the bottom, more momentum is carried by smaller eddies than farther from the bottom. Any flow sensor has a sampling volume, and if close to the bottom, the sensor will average away the smaller eddies carrying some of the stress, causing the sensor to under measure that stress. A second potential cause of lowered covariance stress of the lowest sensor is form drag. The upstream one-meter-high sand waves may have had form drag which might not be fully measured below their one-meter height. Many researchers have attributed more stress to form drag than skin friction [18]. The bottom BASS sensor, at 39 centimeters above bottom with a 15 centimeter-long measurement volume, did measure less stress than the higher sensors due to averaging of some of the stress carrying eddies, and possibly also due to form drag not present at this height.

In a tidally driven shallow flow ignoring wind stress, one expects the stress to vary linearly from the bottom to

$$\tau(z) = \tau_b(1 - \frac{z}{h}) \quad (3)$$

zero at the top surface. In equation (3), τ is the shear stress at a height above bottom of z, τ_b is the bottom shear stress, and h is the total water depth. The mean covariance stresses were compared to this. The drag-law, log-fit, and inertial-dissipation stress estimates were compared to the bottom stress. The wall region usually extends up to 15-20% of the mean flow depth or 0.03-0.04*u_*/ω whichever is smaller, ω is the tidal frequency. In this flow, the top of the wall region is expected to be from 2.3 to 3.1 meters above bottom so the top sensor at 3.08 meters is at the upper limit of the wall region and may be entering the wake region [19, 14]. With the top sensor at just over three meters above bottom in 15.6 meters of water, the stress at the top sensor should have been twenty percent less than the bottom stress. The log-fit, drag-law, and inertial dissipation estimates used assume a constant-stress wall layer and could be in error by as much as twenty percent for the top sensor and seven percent for the middle sensor.

The log-fit stress estimate is made by fitting mean velocities at the different sensor heights above bottom to a logarithmic layer model [20]. In equation (4) $\bar{u}$ is the mean

$$\frac{\bar{u}}{u_*} = \frac{1}{\kappa}\ln(\frac{z-d}{h_o}) + B \quad (4)$$

velocity at height z, u_* is the friction velocity defined to be the square root of the shear stress divided by density, κ is von Karman's constant taken to be 0.4, d is a displacement height, h_o is the roughness scale, and B is an empirical function of the roughness Reynold's number. Log-fit stress estimates require that equilibrium exists and the boundary layer flow is fully developed over the sensors. The top sensor will lag and may not represent the stress accurately during the flow's tidal acceleration. The log-fit stress estimate requires currents from at least three heights to compute the stress and displacement height. The log-fit stress estimate would have been better by fitting to current measurements at more heights. This paper uses the relation by Gross and Nowell [4] for the confidence interval of the friction velocity estimate. The confidence interval has a t-

$$u_* \pm u_* t_{(n-2;1-1/2\alpha)} \sqrt{\frac{\frac{1}{r^2} - 1}{n-2}} \quad (5)$$

distribution with n-2 degrees of freedom where n is the number of current meter heights and r^2 is the regression coefficient (squared) of the least squares fit. This relation shows that the confidence interval is greatly improved by measuring current at more heights. The displacement height for each seven-minute or half-hour record had so much scatter as to be unusable. In processing, means from the entire deployment were used to calculate the displacement height, which was assumed to be constant. All the log-fit stress estimates were plotted, even when the r^2 regression coefficient was low. Seven-minute velocity means, from the three heights, were used to calculate the friction velocity and stress, which were then averaged with a one-half hour, zero-phase filter.

The inertial dissipation stress estimate is often used to measure wind stress in air and is less sensitive to errors in sensor attitude than the other estimates. If we assume a constant-stress, unstratified, turbulent boundary layer, the shear should be given by

$$\frac{\partial \bar{u}}{\partial z} = \frac{u_*}{\kappa z} \quad (6)$$

In equation (6) $\frac{\partial \bar{u}}{\partial z}$ is the mean velocity shear, u_* is the friction velocity, κ is von Karman's constant, and z is distance from the bottom. If we assume a local balance between generation and dissipation of turbulent kinetic energy, equation (7) will follow.

$$\frac{\tau}{\rho}\frac{\partial \bar{u}}{\partial z} = \varepsilon \quad (7)$$

In equation (7) τ is the shear stress, ρ is fluid density, and ε is the dissipation of turbulent kinetic energy. The dissipation can be measured by fitting the measured wave number velocity autospectra to the inertial dissipation spectrum (8)[5, 21]. In equation (8)

$$\Phi_{11}(k_1) = \alpha_1 \varepsilon^{\frac{2}{3}} k_1^{\frac{-5}{3}} \quad (8)$$

$\Phi_{11}(k)$ is the velocity auto-spectrum in wavenumber space, k_1 is the radian wavenumber in the along current direction, α_1 is the Kolmogorov constant taken to be 0.5, and ε is the dissipation. Temporal frequency velocity auto-spectra were computed and converted to wavenumber spectra using Taylor's frozen turbulence hypothesis.

These equations combine such that the friction velocity is given by

$$u_* = (\frac{\Phi_{11}(k_1) k_1^{\frac{5}{3}}}{\alpha_1})^{\frac{1}{2}} (\kappa z)^{\frac{1}{3}} \quad (9)$$

In equation (9) k_1 is the wave number in the along current direction and κ is von Karman's constant. The friction velocity and therefore stress was computed in 7 minute 20

second periods by fitting this relation. When the frozen turbulence test failed, that is when the standard deviation of velocity was greater than half the mean velocity, the inertial-dissipation stresses were deleted. These periods were at slack tide and occurred less than 7 % of the total record. Because of the breaks in these records, these series were not low-pass filtered.

The turbulent quantities that were calculated are the turbulent kinetic energy generation by mean shear and dissipation. The generation and dissipation are defined in the turbulent kinetic energy equation. In equation (10) the primed

$$(\frac{\partial}{\partial t}+\bar{u}\frac{\partial}{\partial x}+\bar{w}\frac{\partial}{\partial z})\frac{1}{2}q'^2=-\overline{u'w'}\frac{\partial \bar{u}}{\partial z}-\frac{g}{\rho_o}\overline{\rho'w'} -\frac{\partial}{\partial z}(\frac{\overline{p'w'}}{\rho}+\frac{1}{2}\overline{q'^2w'})-\varepsilon \qquad (10)$$

quantities are the fluctuating parts and the over-bar quantities are the mean parts of the variables. The $\frac{1}{2}q'^2$ term is the turbulent kinetic energy divided by density. The terms on the left are the time-rate-of change and horizontal and vertical advection of turbulent-kinetic energy. The first term on the right is the production of turbulent energy by mean shear working on shear stress. The second term on the right is work needed to move heavy fluid up, i.e. mixing of stratified fluid. The third and forth terms on the right are transport of energy by pressure work and diffusion. The last term ε is the dissipation of turbulent energy by viscous dissipation. The terms u and w are velocity in the x and z directions, g is the acceleration due to gravity, ρ is fluid density, and p is pressure.

In the wall equilibrium region of a steady-state, uniform, unstratified boundary layer, the local turbulent energy production and dissipation nearly balance. In equation (10) the terms on the left of the equation are zero by the assumptions of steadiness and uniformity in x and y. The divergence of the convective terms, of pressure transport and turbulent transport, of kinetic energy are much smaller than the local production and dissipation. The mixing of stratified fluid is zero for unstratified flows. The measurements of generation and dissipation will test whether the mixing of stratification may be important.

The generation of turbulent kinetic energy was computed as the product of the seven-minute covariance Reynolds stress and the seven-minute mean shear. The mean shear was a log-fit to the three current measurements. These were then averaged with a one-half hour, zero-phase filter. The log-fit shear for the bottom and top sensors are in fact extrapolations, but the computed quantities are consistent.

The dissipation of turbulent-kinetic energy was calculated by fitting the measured wave-number velocity autospectra to the inertial-dissipation spectrum [5, 21](8). When the frozen turbulence test failed, that is when the standard deviation of velocity was greater than half the mean velocity, the dissipation estimates were deleted. These periods were at slack tide and occurred less than 7 % of the record. The dissipation estimates were then interpolated over these periods in contrast to the inertial-dissipation stresses calculated using the same velocity spectra and requiring the same frozen turbulence test, which were not. This difference in treatment is ad hoc, interpolating the dissipation produced reasonable looking time series, but interpolating inertial dissipation stress did not. The interpolated dissipation time series was then averaged with a one-half hour, zero-phase, low-pass filter.

The lowest BASS sensor was not used to estimate dissipation as its turbulent Reynolds number (the product of the friction velocity, von Karman's constant, and distance from the bottom divided by the kinematic viscosity) was not large enough for an inertial subrange to exist. The inertial dissipation subrange model assumes a large separation of spatial scales from production to viscous dissipation. When the turbulent Reynolds number is too low and the velocity measuring volume too large, this algorithm will under-measure dissipation. If this restriction is ignored, and the dissipation using the lowest sensor is blindly calculated, the calculated dissipation is significantly lower than wall-layer model predictions.

RESULTS

Turbulent shear stress was estimated by the drag-law, covariance, log-fit, and inertial dissipation methods and time series of these estimates are shown in the top graphs of Figs. 3 and 4. The top graph of Fig 3 shows a typical period when the four estimates agreed most of the time. Recall that the inertial dissipation stress is plotted in seven-minute means, when Taylor's frozen turbulence hypothesis test was met, and the other stress estimate plots are continuous and were averaged with a half-hour low-pass filter. Comparing seven-minute inertial dissipation stress to the seven-minute covariance stress shows similar sampling variability of the estimates. The covariance estimates and drag-law estimates from each sensor (logarithmically corrected for height) agreed well both in the mean and in fluctuations. The 95% confidence interval from statistical variability for the seven-minute mean flow was +/- 8%, covariance stress +/- 60%, and inertial dissipation stress +/- 50%. The 95% confidence interval from statistical variability for the half-hour averages of current +/- 4% and covariance stress +/- 30%. The 90% confidence interval from statistical variability using (5) for the half best log-fits for

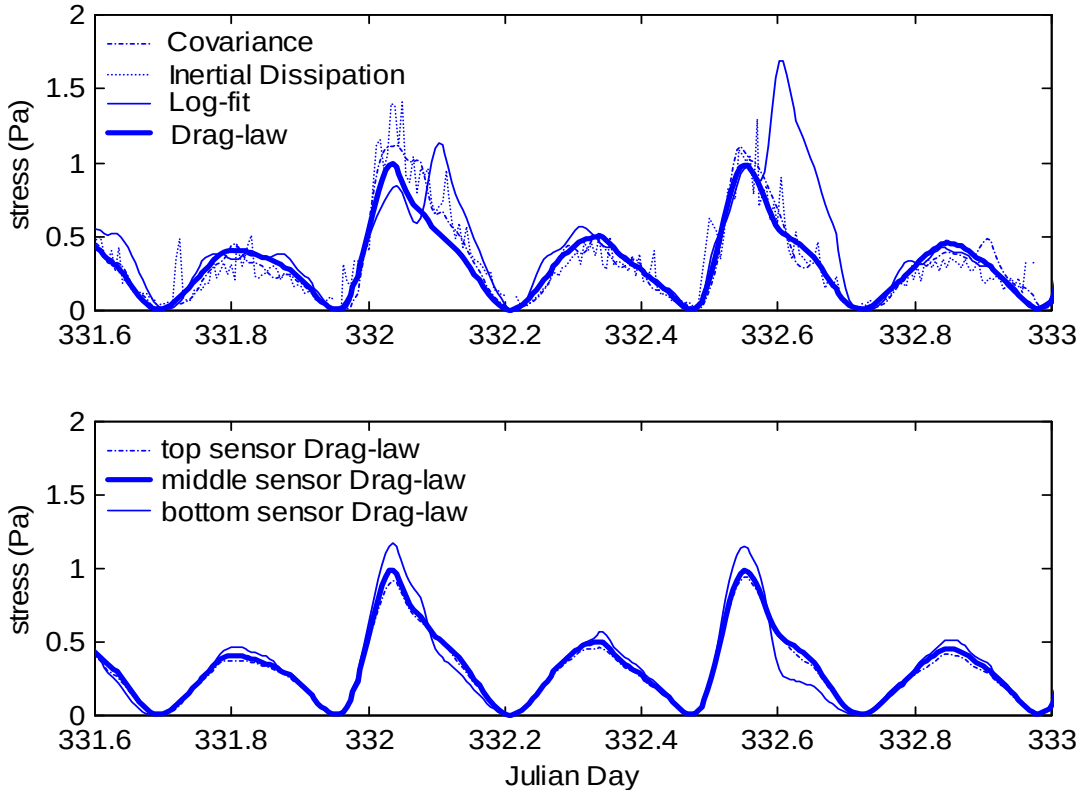

Fig. 3. Time series of stress estimates from drag-law, covariance, log-fit, and inertial dissipation methods. The period in the top graph when the log-fit stress diverged from the other estimates corresponds to a period of reduced measured flow by the bottom sensor, shown by the lowered bottom sensor drag-law stress.

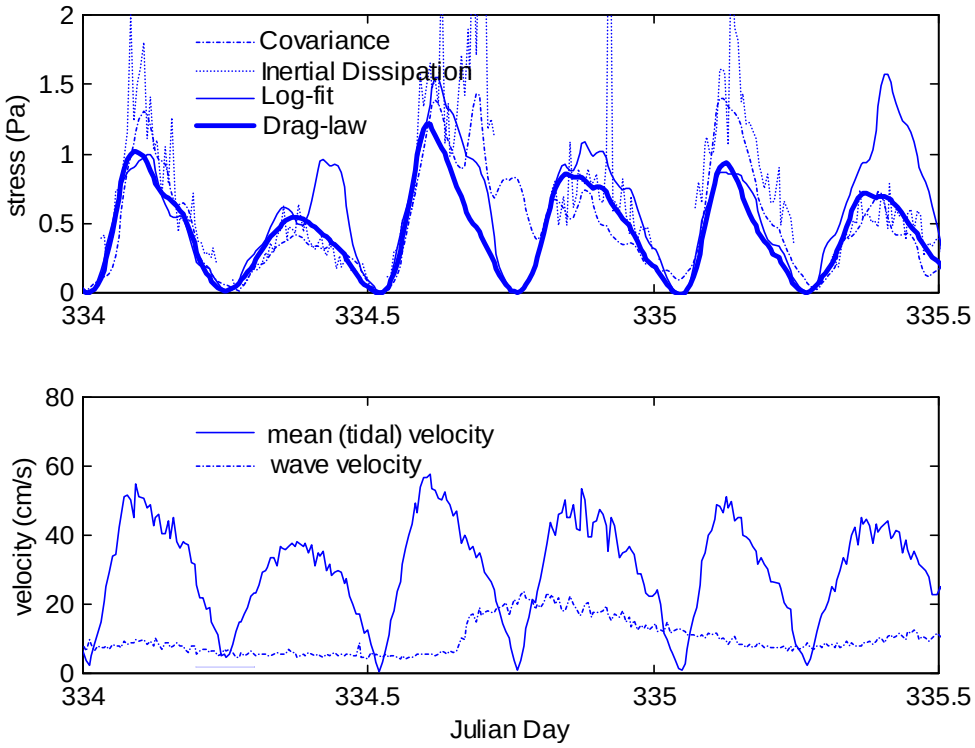

Fig. 4. The top graph is a time series, during a storm, of stress estimates from the drag-law, covariance, log-fit, and inertial dissipation methods. The lower graph is a time series of mean velocity (mostly tidal) and wave velocity. During the peak of the largest storm the covariance stress estimate diverged from the other estimates when the wave velocity was more than four times the mean velocity.

seven-minute stress was a large +256%/-87% showing the need for more measurement heights.

Although within the large confidence interval, there were periods in the record when the log-fit stress estimate diverged from the other stress estimates. The lower graph in Fig. 3 shows the drag-law stress from the three sensors plotted over the same period. The periods when the log-fit stress estimate diverged correspond to lowered measured velocity in the bottom sensor, as shown by its lowered measured drag-law stress. The cause of this non-constant retarded flow in the lowest sensor could have been seaweed draped around the sensor or an upstream bedform that moved during the deployment. An upstream bedform can cause form drag that may not exist as a shear stress at the bottom. An elevated log-fit estimate could have been caused by stable stratification, which would have increased the velocity shear for the same shear stress. This period did have elevated optical backscatter. Stratification would have elevated the mean velocity at the middle and upper sensors elevating their measured drag-law stresses. The drag-law stresses from these upper sensors followed the covariance stress, did not blow up like the log-fit stress, thus indicating that stable stratification was not the cause of the log-fit estimate's divergence.

There was one period, during the largest storm, when the covariance stress estimate diverged from the other estimates and appears to be in error. Recall that in the presence of waves, the covariance estimate can be swamped if the sensor attitude or slope of the bottom is not accurately known and compensated for. The top graph of Fig. 4 is a time series, during this storm of stress estimates from the drag-law, covariance, log-fit, and inertial-dissipation methods. The record around Julian day 334.7 is the only period when the covariance stress diverged from the other estimates. The bottom graph of Fig. 4 shows the mean velocity (mostly tidal) and the wave velocity for the same period. The wave velocity computed here was the standard deviation of the band-pass-filtered velocity with the pass-band being the frequency range over which swell reached the bottom. When the wave velocity exceeded four times the mean velocity the covariance estimate diverged from the other estimates and appears erroneous.

Seven-minute means of drag-law stress are compared to the one-half hour covariance stress estimates on a scatter plot in Fig. 5. These drag-law stress estimates assumed a constant drag coefficient for the entire deployment. These stress estimates are well correlated. The correlation coefficient between the seven-minute drag-law estimates and the half-hour covariance estimates was 0.91 while the correlation coefficient between the half-hour drag-law and covariance estimates was 0.92.

In order to check how the drag coefficient varies with wave activity, the drag coefficient was calculated from the half-hour means of covariance stress and mean velocity. The calculated drag coefficient is plotted, in a scatter plot, as a function of the ratio of wave velocity over current velocity in Fig. 6. The data shown are the records when the current exceeded 5 cm/s, which was 95% of the entire deployment. A least squares fit to this data gives a drag coefficient equal to $0.0021 + 0.014*U_{wave}/U_{current}$ with a correlation coefficient of 0.62.

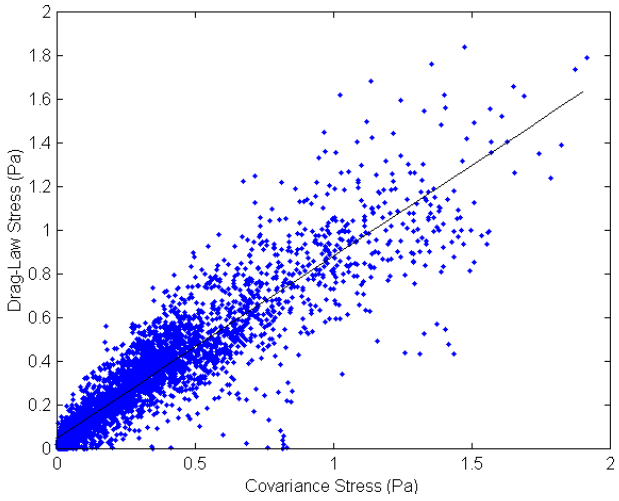

Fig. 5. Scatter plot of seven-minute means of drag-law stress to the half-hour means of covariance stress both from the middle sensor, showing good correlation.

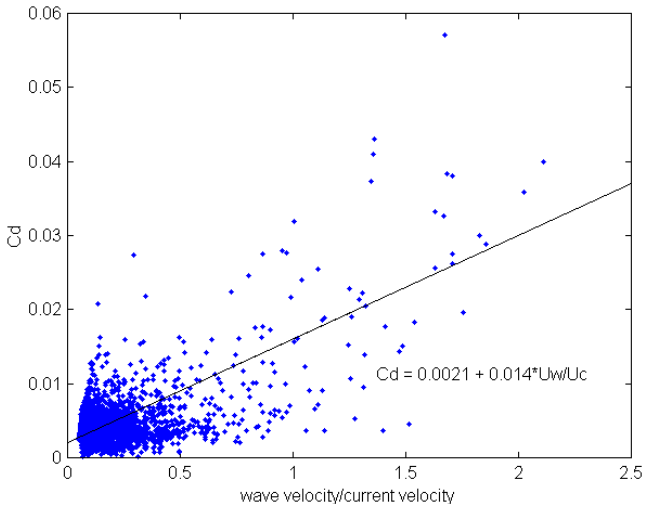

Fig. 6. Scatter plot of half-hour computed drag coefficient from the covariance stress and mean velocity plotted as a function of the wave velocity divided by the current, when the current exceeded 5 cm/s.

The log-fit stress is compared to the covariance stress estimates in Fig. 7. The correlation coefficient of the half-hour means of log-fit and covariance stress was 0.62. There were several periods when the log-fit stress was much larger than the other estimates of stress. As mentioned above, these periods of excessive log-fit stress could have been caused by retarded flow in the lowest sensor. When log-fit stress estimates differencing the top and bottom sensors are compared to the log-fit stress differencing the middle and bottom sensors were compared, the correlation coefficient was 0.85 showing significant sampling variability between different log-fit estimates. Better log-fit stress estimates can be made by fitting to currents measured at more than three heights.

The excess log-fit over covariance stress was compared to the pressure standard deviation and optical backscatter. Presence of waves increases turbulence in the bottom-boundary layer increasing the turbulent diffusivity, which should result in the log-fit estimate under-estimating stress. The pressure standard deviation is a measure of wave activity on the bottom. The correlation coefficient of the log-fit minus the covariance stress with the pressure standard deviation was –0.1, which is consistent with the theory but hardly a strong correlation. Stable stratification inhibits vertical-turbulent diffusivity and the optical-backscatter sensors are a measure of the amount of sediment in the water column. The correlation coefficient of the excess log-fit over covariance stress with the OBS output was 0.21. This correlation is low but consistent with stable stratification inhibiting turbulence and vertical diffusivity, increasing shear for the same shear stress, causing the log-fit to over-predict stress. The OBS sensors were not calibrated with the local sediment and cannot give a meaningful numerical sediment load or density gradient.

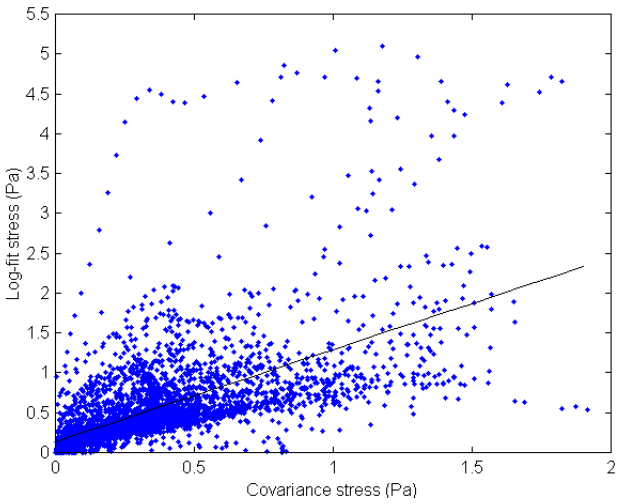

Fig. 7. Scatter plot of half-hour means of log-fit stress to the half-hour means of covariance stress.

The inertial-dissipation stress is compared to the covariance stress in Fig. 8. Both estimates are from the middle sensor. The inertial dissipation estimate is plotted in seven-minute means when the Taylor's-frozen-turbulence-hypothesis test was met. The covariance stress estimate was averaged with a half-hour, low-pass filter and is plotted for the same periods. The mean inertial-dissipation stress for the middle sensor when it was good was 16 % larger than the mean covariance stress for the same periods. The correlation coefficient for these estimates was 0.81.

The mean magnitudes of the stress estimates are compared, in Table 1, to the covariance estimate from the middle sensor and scaled by the linear-tidal-shear stress assumed in equation (3). The mean covariance stress of the low velocity sensor at 39.4 centimeters above bottom was 37% below the mean middle-sensor's covariance stress extrapolated by (3). This was due to averaging of the small

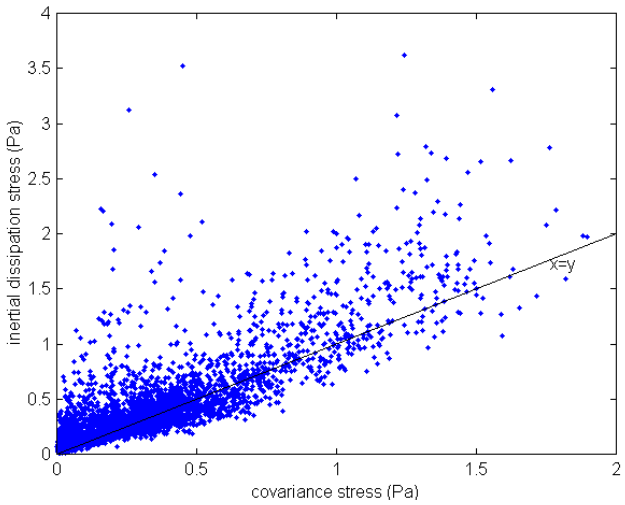

Fig. 8. Scatter plot of seven-minute means of inertial dissipation stress to half-hour means of covariance stress.

TABLE 1

STRESS MEANS

Sensor	Covariance	Drag-law	Log-Fit	Inertial Dissipation
Top	-11%	-2.6%	---	+40%
Middle	---	---	+11%	+16%
Bottom	-37%	+0.3%	---	-27%

stress carrying eddies and possibly an upstream bedform. The mean covariance stress of the top sensor was 11%below the extrapolated middle-sensor covariance stress. This could be the result of the tidal-boundary layer, at 3 meters above bottom, not being fully developed. The drag coefficient from fitting the middle sensor drag-law stress to the covariance stress was $4.1 * 10^{-3}$, which is larger than the $2\text{-}3 * 10^{-3}$ usually mentioned in the literature for current with no waves and is within the range for current with waves. This boundary layer was unstratified, the bottom did have ripples, and swell was present at the bottom during much of the deployment. The drag-law mean, using the same drag coefficient and scaling the velocity to a log profile, from the top sensor was 3% below that of the middle sensor while the low sensor drag-law mean was 0.3% higher than that of the middle sensor. The log-fit bottom stress mean was 11% higher than the bottom stress from the middle sensor covariance mean. The bottom sensor underestimated inertial dissipation stress by 27 % because its turbulence Reynolds number was too low for an inertial subrange to exist and the bottom sensor averaged down the smaller eddies due to its large sampling volume relative to its distance from the bottom. If the Huntley correction [21] is applied to the bottom-sensor inertial-dissipation stress estimate, it is still 11 % low. The top two sensors had an adequate turbulent Reynolds number and do not need the Huntley correction. The top-sensor inertial-dissipation stress was significantly larger than the other stress estimates, which the authors do not fully understand.

One hypothesis for the elevated inertial-dissipation stress of the top sensor is extra turbulence created by wakes of the tripod and or sensor. The tripod and sensors were designed to minimize flow disturbance, but especially in waves where the sensor and tripod wakes can be advected back into the sensing volume, there could have been some wake-generated turbulence. The inertial-dissipation stress model assumes the dissipation to follow a one-over-distance-from-the-bottom profile. A little added dissipation upwardly biases an inertial-dissipation stress estimate from a sensor farther from the bottom more than from a sensor close to the bottom, where the wall-layer dissipation is larger. Additionally, the top sensor was closer to the tripod legs than the lower sensors. Wake generated turbulence may have contributed to the high inertial-dissipation stress estimate of the top sensor.

Tidal asymmetry between current and stress between the accelerating and decelerating portions of the tidal cycles were not obvious for individual cycles but was when the record was tidally averaged. The individual tidal cycles had large statistical variability in measured stress; stress asymmetries varied from cycle to cycle. The records were averaged for 38 semidiurnal tide cycles to reduce the confidence intervals from statistical variability. Statistically significant tidal asymmetry in the covariance, log-fit, and inertial dissipation stress estimates was found and is shown in Fig. 9. for the first half of the averaged semidiurnal cycles. The second half of the cycle had lower velocities and showed less asymmetry. This data is consistent with McLean 83 [3] but more tidal cycles are averaged and separate curves for the three stress estimates are shown. The covariance stress is shown as asterisks during acceleration and circles during deceleration. The log-fit stress is plotted displaced up by a half Pascal and the inertial-dissipation stress by one Pascal. Confidence intervals of 95% in current, covariance stress and inertial-dissipation stress are indicated by the rectangles while the log-fit rectangles show a 90% confidence interval. The drag-law stress with a constant drag coefficient would show zero asymmetry in this plot and was not included. The measured log-fit stress shows more asymmetry during tidal cycles than either the covariance or inertial-dissipation stress estimates. The relatively smaller asymmetry in the inertial-dissipation stress explains why many researchers did not measure statistically significant tidal asymmetry close to the bottom from one or two tidal cycles.

The generation and dissipation of turbulent-kinetic energy were calculated and a short time record of these

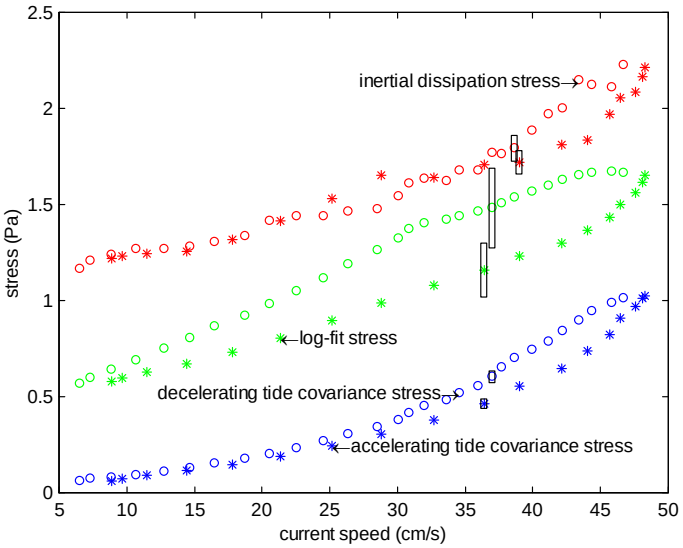

Fig. 9. Current velocity and stress estimates from covariance, log-fit displaced up by 0.5 Pascals, and inertial-dissipation displaced up by 1 Pascal, of the first half of the average of 38 semidiurnal tidal cycles. The rectangles represent the 95% confidence intervals due to statistical variability of current, covariance and inertial dissipation stresses and the 90% confidence interval for the log-fit stress.

measured by the middle sensor is shown in Fig. 10. The 95% confidence interval from statistical variability for the half-hour smoothed TKE generation is +/- 35% and for the dissipation +/- 40%. The generation and dissipation followed each other fairly well, consistent with a local

balance of generation and dissipation assumed in equation (7).

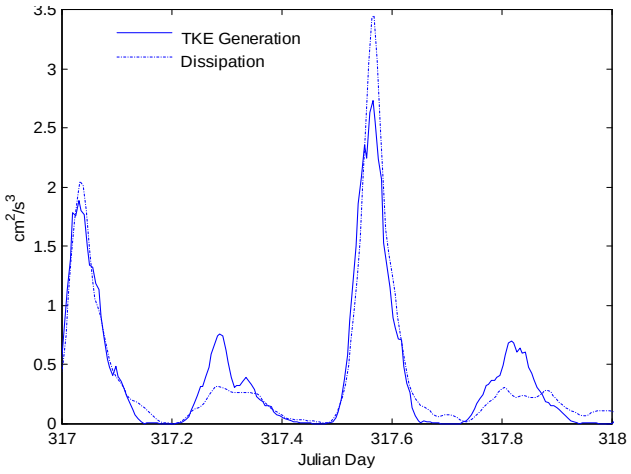

Fig. 10. Time record of half-hour means of turbulent-kinetic energy generated by mean shear and dissipation.

The difference between generation and dissipation was computed to compare to turbulence theory and is plotted in Fig. 11 along with pressure standard deviation and optical backscatter. If waves are present in the bottom-boundary layer, there will be additional TKE generated above that generated by mean stress and mean shear. One expects the dissipation to exceed the TKE generated by mean shear when waves are present. Pressure standard deviation is used as a measure of wave activity. If the bottom-boundary layer is stably stratified, one expects that TKE generation will exceed dissipation, by the energy that goes into the $-\frac{g}{\rho_o}\overline{\rho' w'}$ term of equation (10) that is work required in diapycnal mixing. Comparing the TKE generation by mean shear minus dissipation with pressure standard deviation and optical backscatter measures the effect on turbulence of waves and stratification.

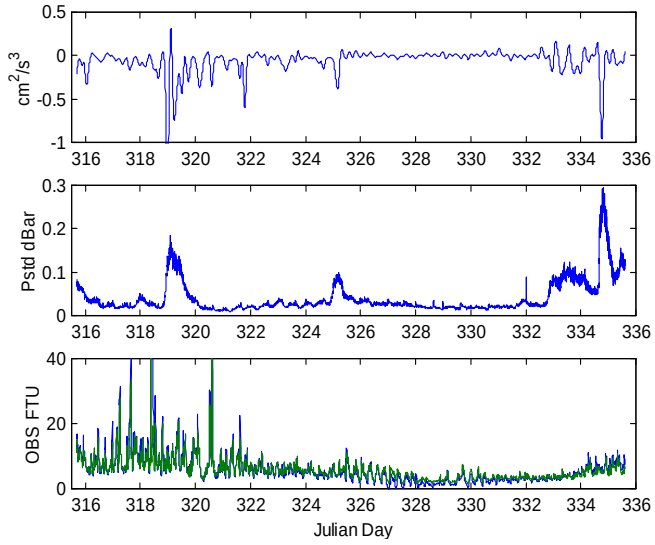

Fig. 11. The top graph is TKE generation minus dissipation in half-hour means for the entire deployment for the top sensor. The middle and bottom graphs show pressure standard deviation, a proxy for waves, and optical backscatter, a proxy for stratification by sediment load. Some negative correlation is seen between the excess TKE and pressure standard deviation.

The excess TKE (generation by mean shear minus dissipation) is shown in a scatter plot with pressure standard deviation in Fig. 12. The correlation coefficient was –0.42 consistent with the idea that wave activity is also generating turbulence, but the magnitude of the correlation is not large.

To test how much TKE generation was consumed by diapynchnal mixing, the TKE excess, of generation minus dissipation, was compared to the OBS record. This correlation coefficient was –0.2 which is not consistent with the expectation that stable stratification from turbidity would consume some of the TKE and make the dissipation less than the TKE generation by mean shear. Two factors appear to contribute to this unexpected result, the optical turbidity is dominated by tiny fine particles that may not contribute significant extra density to the flow and the correlation between waves and turbidity. As described above, the wave boundary layer adds TKE to the current-boundary layer above the amount generated by mean shear. Turbidity is kicked up by waves and is therefore correlated with waves. Apparently the waves add much more TKE to

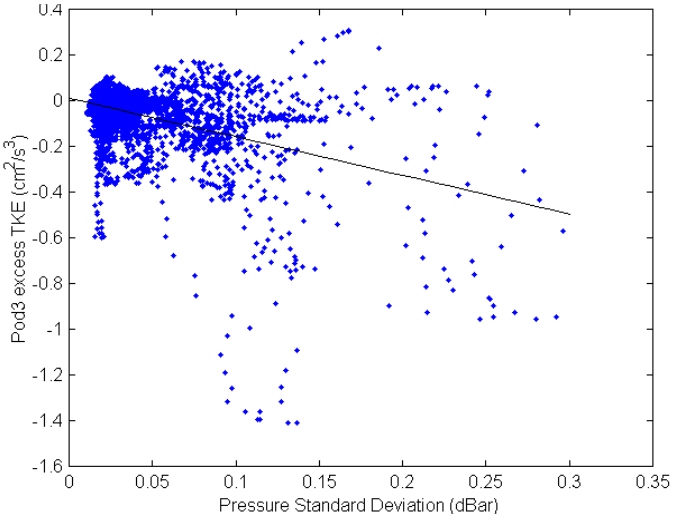

Fig. 12. Scatter plot of TKE generated by mean shear minus dissipation plotted against pressure standard deviation, a measure of wave activity.

the boundary layer than is absorbed by stratification associated with turbidity kicked up by the same waves.

The mean TKE generation and dissipation are compared to a wall-layer model in Fig. 13. The C/z line is the wall-layer prediction of TKE generation with C fitted to the generation of the upper two sensors. The dissipation of the bottom sensor was not plotted. As mentioned above, the turbulence Reynold's number for the bottom sensor was below the value where an inertial dissipation region could be expected. The TKE generation of the bottom pod is plotted and is low, presumably due to the bottom sensor averaging out some of the small eddies carrying momentum. The difference in this measurement from the C/z curve is not, therefore, significant. The mean of the upper two sensor's generation and dissipation matched to within one percent. The generation of the middle sensor was higher than its dissipation, while the dissipation of the top sensor was greater than generation, but these differences were within the standard error. While not statistically significant, these differences are consistent with the flow at sensor 2 adding turbulent energy to the turbulent energy flux away

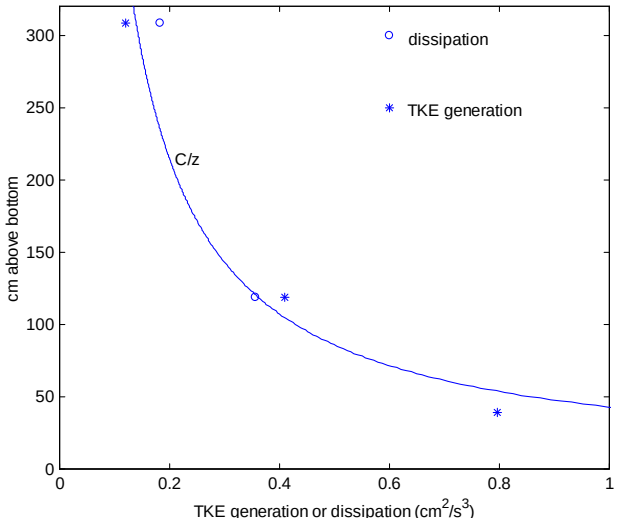

Fig. 13. Means for the entire deployment of TKE generated by mean shear and dissipation. The line is a wall-layer model fitted to the generation of the upper two sensors. The data balances generation and dissipation to within the standard error.

from the bottom and the flow at the higher sensor absorbing some of this energy flux. To within statistical error, the generation and dissipation of turbulent-kinetic-energy balance, and are inversely proportional to the distance from the bottom.

CONCLUSIONS

The data set from the North Sea BASS deployment is useful for testing unstratified-turbulence models. The drag coefficient measured by covariance stress as a function of the ratio of wave to current velocity and the tidally averaged asymmetries of the log-fit, covariance, and inertial dissipation stress estimates are the principal contributions of this paper. Specific observations are summarized below:

The drag-law stress estimate had the lowest sampling variability but suffered from the fact that the drag coefficient varies with a flow's bottom roughness, waves, and stratification. All of these changed over the duration of the deployment.

The covariance estimate had the most sampling variability but was the best of the four estimates for measuring stress in stratified flows. The bottom sensor under-sampled the stress by averaging down the smaller eddies carrying momentum. The higher sensors were not as effected, because farther from the wall, the momentum carrying eddies are larger.

The log-fit stress estimate diverged from the other estimates on occasion possibly due to retarded flow in the lowest sensor. The log-fit stress estimate would be improved by measuring current at more measurement heights. The log-fit estimate should over-measure stress in stably stratified boundary layers. The log-fit estimate is biased by growth of the boundary layer in accelerated flows and fails to decay rapidly in decelerated flows.

The inertial-dissipation stress estimates had almost as large a sampling variability as the covariance estimates and could not estimate stress at slack tide. The bottom sensor underestimated inertial-dissipation stress because it was so close to the bottom that its turbulence Reynolds number was too low for an inertial subrange to exist and because it was too close to the bottom for its sample volume. The top sensor inertial-dissipation stress was significantly larger than the other stress estimates.

Averaging 38 semidiurnal tide cycles together showed stress asymmetry between the accelerating and decelerating portions. This asymmetry was largest using the log-fit estimate and smaller using the covariance and inertial-dissipation stress estimates.

The measured turbulent energy generation and dissipation balanced to within statistical error for the two higher sensors and followed the inverse height above bottom dependence predicted for unstratified wall layers. The lowest pod under-measured both dissipation and generation.

SUMMARY

Tidal boundary layers subject to waves and stratification present opportunities to compare estimates of stress based on different statistical measures. The data acquired in the North Sea that are presented here illustrate the characteristics and utility of the methods of

covariance, log-fit, inertial dissipation, and drag law for estimating stress.

REFERENCES

[1] Bowden, K. F. and M. R. Howe, "Observations of turbulence in a tidal current," J. Fluid Mech., Vol. 17, pp. 271-284.

[2] Sternberg, R. W., "Friction Factors in Tidal Channels with Differing Bed Roughness," Marine Geology, Vol. 6, pp. 243-260, 1968.

[3] McLean, S. R. "Turbulence and Sediment Transport Measurements in a North Sea Tidal Inlet (The Jade)," *North Sea Dynamics* Stringer-Verlag, pp. 436-452, 1983.

[4] Gross, T. F. and A. R. M. Nowell, "Mean flow and turbulence scaling in a tidal boundary layer," Continental Shelf Res. Vol. 2, Nos 2/3, pp. 109-126, 1983.

[5] Gross, T. F. and A. R. M. Nowell, "Spectral Scaling in a Tidal Boundary Layer," JPO, Vol. 15, pp. 496-508, 1985.

[6] Gross, T. F., A. J. Williams, and E. A. Terray, "Bottom boundary layer spectral dissipation estimates in the presence of wave motions," Continental Shelf Res. Vol. 14, No. 10/11, pp. 1239-1256, 1994.

[7] Sanford, T. B. and Ren-Chieh Lien, "Turbulent properties in a homogeneous tidal bottom boundary layer," JGR, Vol. 104, No. C1, pp. 1245-1257, 1999.

[8] Wolf, J., "Estimation of shearing stresses in a tidal current with application to the Irish Sea," *in Marine Turbulence*, edited by J. Nihoul, Elsevier Sci., New York, pp. 319-344, 1980.

[9] Bowden, K. F. and S. R. Ferguson, "Variation with height of the turbulence in a tidally-induced bottom boundary layer," in *Marine Turbulence*, edited by J. Nihoul, Elsevier Sci., New York, pp. 258-286, 1980.

[10] Soulsby, R. L. and K. R. Dyer, "The form of the near-bed velocity profile in a tidally accelerating flow," JGR, Vol. 86, No. C9, pp. 8067-8074, 1981.

[11] Gross, T. F., A. E. Isley, and C. R. Sherwood, "Estimation of stress and bed roughness during storms on the northern California shelf," Continental Shelf Res. Vol. 12, No. 2/3, pp. 389-413, 1992.

[12] Green, M. O. and I. N. McCave, "Seabed drag coefficient under tidal currents in the eastern Irish Sea," JGR, Vol. 100, No. C8, pp. 16,057-16,069, 1995.

[13] Simpson, J. H., W. R. Crawford, T. P. Rippeth, A. R. Campbell, and J. V. S. Cheok, "The vertical structure of turbulent dissipation in shelf seas," JPO, Vol. 26, pp. 1579-1590, 1996.

[14] Lueck, R. G. and Y. Lu, "The logarithmic layer in a tidal channel," Continental Shelf Res. Vol. 17, No. 14, pp. 1785-1801, 1997.

[15] Williams, A. J. 3rd, J. S. Tochko, R. L. Koehler, W. D. Grant, T. F. Gross, and C. V. R. Dunn, "Measurement of Turbulence in the Oceanic Bottom Boundary Layer with an Acoustic Current Meter Array," J. Atmos. And Oceanic Tech. Vol. 4, pp. 312-327, 1987.

[16] Grant, W. D., A. J. Williams 3rd, and S. M. Glenn, "Bottom Stress Estimates and their Prediction on the Northern California Continental Shelf during CODE-1: The Importance of Wave-Current Interaction," JPO, Vol. 14, pp. 506-527, 1984.

[17] Heathershaw, A. D. and J. H. Simpson, "The Sampling Variability of the Reynolds Stress and its Relation to Boundary Shear Stress and Drag Coefficient Measurements," Estuarine and Coastal Marine Science Vol. 6, pp. 263-274, 1978.

[18] Chriss, T. M. and D. R. Caldwell, "Evidence for the influence of form drag on bottom boundary layer flow," JGR, Vol. 87, No. C6, pp. 4148-4154, 1982.

[19] Lopez, F. and M. H. Garcia, "Wall Similarity in Turbulent Open-Channel Flow," J. of Eng. Mech. pp. 789-796, July 1999.

[20] Monin, A. S. and A. M. Yaglom, *Statistical Fluid Mechanics* MIT Press, pp. 257-364, 1971.

[21] Huntley, D. A., "A Modified Inertial Dissipation Method for Estimating Seabed Stresses at Low Reynolds Numbers, with Application to Wave/Current Boundary Layer Measurements," JPO, Vol. 18, pp. 339-346, 1988.